JOURNAL OF MAGNETIC RESONANCE **125,** 348–354 (1997)
ARTICLE NO. MN971112

NOTES

Artifact-Free Pure Absorption PFG-Enhanced DQF-COSY Spectra Including a Gradient Pulse in the Evolution Period

BERNARD ANCIAN,* ISABELLE BOURGEOIS,† JEAN-FRANÇOIS DAUPHIN,† AND ANTHONY A. SHAW†,‡

**Department of Chemistry, Université Paris 7, 2 Place Jussieu, 75251 Paris Cedex 05, France; and †Bristol-Myers Squibb Company, Pharmaceutical Research Institute, Centre de Recherche et de Production, Rue de la Maison Rouge, B.P. 62, 77422 Marne-la-Vallée Cedex, France*

Received October 11, 1996; revised December 30, 1996

We have recently shown that artifacts due to rapid pulsing in gradient-enhanced double-quantum-filtered (GEDQF) homonuclear COSY experiment can be suppressed by a suitable choice of gradients during evolution, mixing, and detection periods (*1*). The proposed combination 4:3:10 blocks multiple-quantum coherences generated during the evolution period. However, by retaining only one coherence pathway (N or P), the application of the first gradient leads to two major drawbacks: (i) a reduction in sensitivity by a factor of two and (ii) the inability to obtain pure-phase double-absorption spectra (*2, 3*).

Whereas the loss in sensitivity is not a critical defect, the phase-twist lineshape may be a severe handicap in high-resolution NMR because of the increased linewidth generated by the magnitude calculation mode and the loss of information about the signs of the cross peaks. J. Keeler *et al.* (*3*) have recently shown that the key to retaining both coherences (+1 and −1) during t_1, and thus to obtaining time-domain data which are amplitude modulated in t_1 and can be phased along the ω_1 dimension, is not to apply a gradient during the evolution period. It is unfortunately clear that this modification is fundamentally incompatible with a complete removal of multiple-quantum rapid-pulsing artifacts generated by the first 90° pulse which requires the unavoidable application of a gradient immediately after the preparation period.

Another original idea called the *sw*itched *a*cquisition *t*ime (SWAT) gradient method has been proposed by Hurd *et al.* (*4*). It consists of sampling the time-domain signal at twice the dwell rate, inserting appropriate alternating positive and negative gradient pulses between digitized points for encoding coherence pathways $0 \rightarrow -1 \rightarrow -1$ (P type) and $0 \rightarrow +1 \rightarrow -1$ (N type) in a single acquisition. While this method avoids collection of additional data blocks, in contrast to the traditional RF phase cycling (*5–8*), it results in a Nyquist frequency shift in the ω_2 dimension for the sine-modulated components compared to cosine-modulated ones. Although data reconstruction and processing are extremely simple, the gradient-switching time and the recovery from eddy-current effects limit the maximum digitization rate and hence the spectral bandwidth in the acquisition dimension. Thus, suffering from such severe instrumental constraints, this elegant solution has not yet been routinely implemented on modern high-resolution spectrometers.

In another key paper, the Keeler group (*9*) has described a simple method for obtaining pure-absorption heteronuclear correlation spectra with the aid of carefully placed pulsed field gradients in the pulse-sequence timing. The idea is to record two separate spectra with gradients of the same magnitude, but with alternately positive (negative) and negative (positive) signs. In the first spectrum, suitable gradients select the N type or echo spectrum (coherence order +1 during t_1 and −1 during t_2), whereas in the second spectrum, another gradient sequence selects the P type or antiecho spectrum (coherence order −1 during t_1 and −1 during t_2). Although each of these spectra will show the undesirable phase-twist lineshape, they can always be combined during data processing to yield a pure-absorption-mode spectrum (*10, 11*). Nevertheless, such an attractive alternative has not yet been used in homonuclear correlation even though phase errors due to the evolution of chemical shifts during the first gradient are certainly less severe than in heteronuclear spectroscopy.

In this Note, we propose a variant of the Keeler method (*9*) with much simpler data manipulation and processing. The signals from P-type and N-type pathways are alternately collected and added in the same data block, time-domain filtered in both dimensions, and Fourier transformed as a complex signal in the t_2 domain and as a real signal in the t_1 domain according to the time-proportional phase-incrementation (TPPI) scheme (*11–13*). Finally, the spectra are phased by standard procedures, and it is shown that the first few data points of the FIDs, which have been corrupted by

‡ To whom correspondence should be addressed.

1090-7807/97 $25.00

the first gradient in the evolution period and preclude clean phasing along ω_1, can be easily recalculated by backward linear prediction (LP) (*14–17*). This method had the clear advantage of providing pure-phase spectra without rapid-pulsing artifacts.

Let us represent a typical P peak by the time-domain expression

$$S_{\mathrm{P}}(t_1, t_2) = \exp[i(\omega_1 t_1 + \varphi_1)]\exp\left(-\frac{t_1}{T_2^{(1)}}\right) \times \exp[i(\omega_2 t_2 + \varphi_2)]\exp\left(-\frac{t_2}{T_2^{(2)}}\right), \quad [1]$$

where φ_1 and φ_2 are phase deviations, ω_1 and ω_2 are the proton offsets from the pulse carrier frequency ω_0, and $T_2^{(1)}$ and $T_2^{(2)}$ are the (assumed) exponential relaxation times in the t_1 and t_2 periods respectively. The phase deviations are assumed to be frequency dependent according to a linear function of the type

$$\varphi_{1,2} = \varphi_{1,2}^{(0)} + \varphi_{1,2}^{(1)}\omega_{1,2}$$

to include the effects of initial delays, the finite duration of gradient pulses, electronic filters, and mismatching in quadrature detection (*18*). Likewise, a typical N peak will be given by

$$S_{\mathrm{N}}(t_1, t_2) = \exp[-i(\omega_1 t_1 + \varphi_1)]\exp\left(-\frac{t_1}{T_2^{(1)}}\right) \times \exp[i(\omega_2 t_2 + \varphi_2)]\exp\left(-\frac{t_2}{T_2^{(2)}}\right). \quad [2]$$

Adding these two signals in the same data block for all the even t_1^{e} increments gives the amplitude cosine-modulated function $S_{\mathrm{C}}(t_1^{\mathrm{e}}, t_2)$

$$\begin{aligned} S_{\mathrm{P}}(t_1^{\mathrm{e}}, t_2) + S_{\mathrm{N}}(t_1^{\mathrm{e}}, t_2) &= S_{\mathrm{C}}(t_1^{\mathrm{e}}, t_2) \\ &= 2\cos(\omega_1 t_1^{\mathrm{e}} + \varphi_1) \\ &\quad \times \exp\left(-\frac{t_1^{\mathrm{e}}}{T_2^{(1)}}\right) \\ &\quad \times \exp[i(\omega_2 t_2 + \varphi_2)] \\ &\quad \times \exp\left(-\frac{t_2}{T_2^{(2)}}\right). \end{aligned} \quad [3]$$

Complex Fourier transformation of [3] with respect to t_2 generates the even interferogram

$$S_{\mathrm{C}}(t_1^{\mathrm{e}}, \omega_2) = 2\cos(\omega_1 t_1^{\mathrm{e}} + \varphi_1)\exp\left(-\frac{t_1^{\mathrm{e}}}{T_2^{(1)}}\right) \times [A_2(\omega_2) + iD_2(\omega_2)]\exp(i\varphi_2), \quad [4]$$

where $A_2(\omega_2)$ and $D_2(\omega_2)$ represent, respectively, the pure-absorption- and dispersion-mode Lorentzians (*18*)

$$A_2(\omega_2) = \frac{T_2^{(2)}}{1 + (T_2^{(2)}\Delta\omega_2)^2} \text{ and } D_2(\omega_2) = -\frac{T_2^{(2)}\Delta\omega_2}{1 + (T_2^{(2)}\Delta\omega_2)^2}, \quad [5]$$

where $\Delta\omega_2 = \omega - \omega_2$.

If the phase φ of the first $\pi/2$ pulse preceding the evolution period t_1 is advanced by $\pi/2$, Eq. [1] gives for the next incremented time $t_1 + \Delta t_1$, which is now an odd t_1^0 increment, the following respective P and N peaks

$$\begin{aligned} S_{\mathrm{P}}(t_1 + \Delta t_1, t_2) &= \exp\left\{i\left[\omega_1(t_1 + \Delta t_1) + \frac{\pi}{2} + \varphi_1\right]\right\} \\ &\quad \times \exp\left[-\frac{(t_1 + \Delta t_1)}{T_2^{(1)}}\right] \\ &\quad \times \exp[i(\omega_2 t_2 + \varphi_2)]\exp\left(-\frac{t_2}{T_2^{(2)}}\right) \\ &= i\exp\{i[\omega_1(t_1 + \Delta t_1) + \varphi_1]\} \\ &\quad \times \exp\left[-\frac{(t_1 + \Delta t_1)}{T_2^{(1)}}\right] \\ &\quad \times \exp[i(\omega_2 t_2 + \varphi_2)]\exp\left(-\frac{t_2}{T_2^{(2)}}\right) \end{aligned} \quad [6]$$

$$\begin{aligned} S_{\mathrm{N}}(t_1 + \Delta t_1, t_2) &= \exp\left\{-i\left[\omega_1(t_1 + \Delta t_1) + \frac{\pi}{2} + \varphi_1\right]\right\} \\ &\quad \times \exp\left[-\frac{(t_1 + \Delta t_1)}{T_2^{(1)}}\right] \\ &\quad \times \exp[i(\omega_2 t_2 + \varphi_2)]\exp\left(-\frac{t_2}{T_2^{(2)}}\right) \\ &= -i\exp\{-i[\omega_1(t_1 + \Delta t_1) + \varphi_1]\} \\ &\quad \times \exp\left[-\frac{(t_1 + \Delta t_1)}{T_2^{(1)}}\right] \\ &\quad \times \exp[i(\omega_2 t_2 + \varphi_2)]\exp\left(-\frac{t_2}{T_2^{(2)}}\right). \end{aligned} \quad [7]$$

Adding these two signals in the same data block for all the odd t_1^0 increments gives now the amplitude sine-modulated function $S_S(t_1^0, t_2)$

$$\begin{aligned} S_P(t_1^0, t_2) + S_N(t_1^0, t_2) &= S_S(t_1^0, t_2) \\ &= -2 \sin(\omega_1 t_1^0 + \varphi_1) \\ &\quad \times \exp\left(-\frac{t_1^0}{T_2^{(1)}}\right) \\ &\quad \times \exp[i(\omega_2 t_2 + \varphi_2)] \\ &\quad \times \exp\left(-\frac{t_2}{T_2^{(2)}}\right). \end{aligned} \quad [8]$$

Complex Fourier transformation of [8] with respect to t_2 now generates the odd interferogram

$$\begin{aligned} S_S(t_1^0, \omega_2) = -2 \sin(\omega_1 t_1^0 + \varphi_1) \exp\left(-\frac{t_1^0}{T_2^{(1)}}\right) \\ \times [A_2(\omega_2) + iD_2(\omega_2)] \exp(i\varphi_2). \end{aligned} \quad [9]$$

In practice, the cosine- and sine-modulated time-domain data sets [3] and [8] which are interleaved in even and odd t_1 increments are not processed separately, but are left interleaved and complex Fourier transformed with respect to t_2 to give the corresponding interleaved interferograms [4] and [9], respectively (*11*). Then, the data are real Fourier transformed with respect to t_1 according to the usual TPPI scheme (*11–13*), where the time increment $\Delta t_1 = 1/(2\Delta f_1)$ and $\Delta f_1 = \Delta\omega_1/2\pi$ is the required spectral width in ω_1; as a result, only a single absorption-mode line is obtained at $\omega_1 + \Delta f_1$ without any aliased signal in the range $\pm\pi\Delta f_1$ as clearly shown by Keeler and Neuhaus (*11*). Moreover, since the four phase quadrants RR, IR, RI, and II are produced by the two successive Fourier transformations, complete phasing in the two dimensions is possible (*11–13*).

The present method, which inverts the gradient G_1 in the evolution time and adds the data in order to select both P and N pathways, has some analogy with a recent approach proposed in order to phase GE HMQC spectra (*19*). Indeed, Ruiz-Cabello *et al.* (*19*) cycle one of the gradients in two subsequent scans to collect alternatively double-quantum coherence and zero-quantum coherence generated in the evolution period of the HMQC sequence; as they carry opposite phase modulation by the undetected (C^{13}) nuclei, adding them provides the needed amplitude modulation. An important difference exists however. Ruiz-Cabello *et al.* (*19*) cycle the gradient during the detection and not during the evolution period and add the two scans only after Fourier transformation along the t_2 domain has been performed. Our scheme is simpler, both for data acquisition and processing.

Phasing along ω_2, that is, multiplying data by $\exp(-i\varphi_2)$, presents some minor difficulties which can be easily solved by appropriate positioning of refocusing pulses in order to remove dispersion by chemical shifts during fixed delays and gradients (*3, 9*). This is achieved by inserting a 180° pulse and a delay of the same length as the gradient during the mixing time in order to compensate the evolution of the double-quantum coherences present during the first gradient G_1; indeed without this modification, phase properties associated with these coherences are transferred to the observable signals, resulting in complex phase distortions that cannot be removed by conventional phase correction procedures in the ω_2 dimension (*3*). Moreover, since an imperfect 180° pulse can cause arbitrary changes in coherence order, giving rise to unwanted signals in the spectrum (*3*), composite 180° pulse of the type $90^\circ_x 180^\circ_y 90^\circ_x$ (*20*) are preferred to get clean absorption spectra with small baseline distortions. Finally, the relative positions of the second gradient G_2 and this refocusing pulse are of importance, and it is always better to place the gradient after the pulse to ensure the proper selection of the $p = \pm 2$ coherence which have been suitably refocused by the previous pulse (*3, 9*).

In principle, all that remains is to refocus the shift evolution during the penultimate gradient G_2 before the final selection and acquisition. As before, this is done by inserting a delay and a composite 180° pulse, this time of opposite sign to the previous one to again compensate errors in the first. Since acquisition of signal cannot begin until after the last refocusing gradient G_3 and the associated recovery delay, the first part of the FID is lost. As pointed out by Keeler *et al.* (*3*), this is not too severe a constraint, since in DQF COSY all the multiplets are in antiphase so that the detectable signal grows from zero at a rate which is on the order of the J couplings, and the missing signal should be small if the gradient G_3 is short compared to $1/2J_{max}$. This is the case in our study where the gradient pulse widths are 800 μs. The pulse sequence and corresponding coherence-transfer diagram (*18*) for recording pure-absorption GEDQF COSY spectra are shown in Fig. 1.

Spectra were recorded on a Bruker ARX-500 spectrometer equipped with an amplifier capable of generating shaped field-gradient pulses of 50 G/cm. The 5 mm inverse-detection probe used was fitted with a self-shielded gradient coil. The spectral width was set to 5000 Hz in each dimension, with 1024 real and imaginary points in t_2 (acquisition time 0.2 s) and 512 t_1 increments. Four dummy scans and two scans per t_1 increment were made, resulting in a total acquisition time of 21.5 min. The gradient strengths used were 3.5 G/cm per unit. A pure cosine window was used for time-domain filtering in both dimensions prior to 2D Fourier

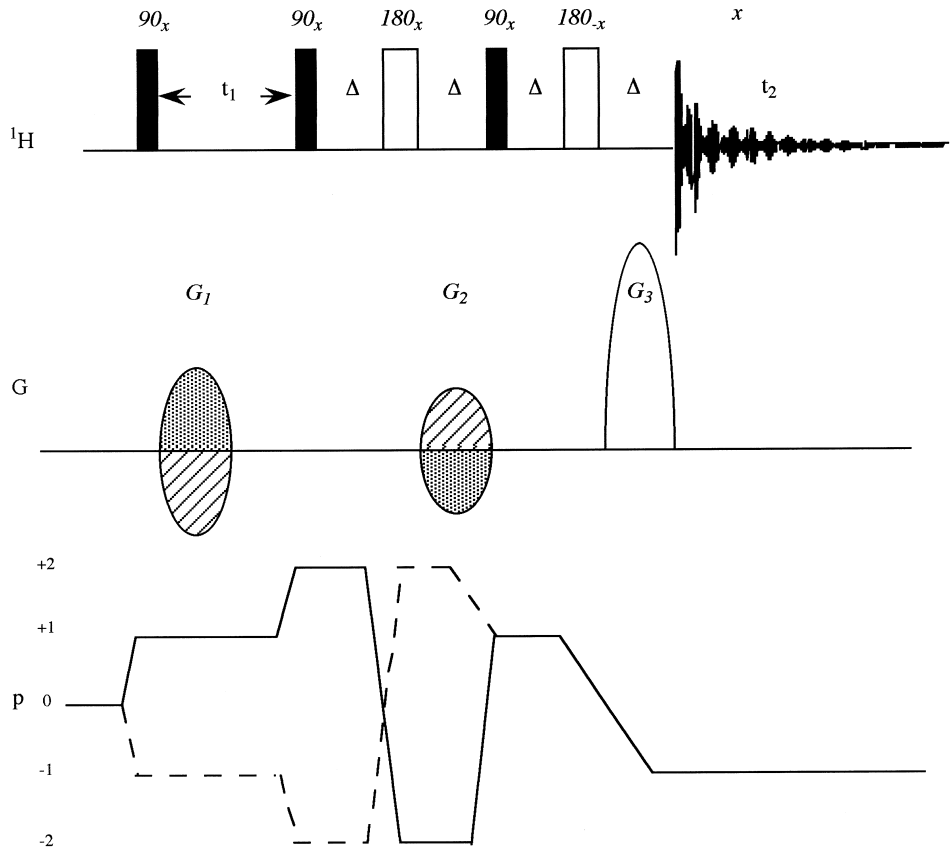

FIG. 1. Pulse sequence, field-gradient timing, and coherence-transfer pathway used to record pure-absorption GEDQF COSY spectra. The delay Δ is constant and equal to the width of the gradient pulses plus associated gradient preparation and recovery times. In our experiments, this was 1.29 ms. For each t_1 increment, the first scan is performed with the 4:−3:10 gradient sequence (dotted), and for the second, the −4:3:10 (hatched) sequence is used. The solid line along the coherence-transfer diagram indicates the pathway $0 \rightarrow +1 \rightarrow +2 \rightarrow -2 \rightarrow +1 \rightarrow -1$ which leads to the N-type spectrum, assuming that the final coherence level $p_5 = -1$ is detected; the dashed line is the ''mirror image'' pathway leading to the P-type spectrum. The RF pulse phases need not be cycled; however, inversion of the signs of the composite π pulses ($90^\circ_x 180^\circ_y 90^\circ_x$ for the first and $90^\circ_{-x} 180^\circ_{-y} 90^\circ_{-x}$ for the second) does appear to give cleaner results.

transformation according to the TPPI procedure. Zero filling was performed once in F_1. The sample was 50 mM 10-desacetylbaccatin III in DMSO-d_6.

Figure 2a shows the complete pure-absorption 2D spectrum, where positive and negative contours have been plotted without distinction. The horizontal cross section along the methylene signals at 2.34 ppm (arrow) indicates phasing along the ω_2 dimension with good-quality antiphase multiplets and reasonably good resolution (Fig. 2b). Unfortunately, a similar cross section along the ω_1 dimension (Fig. 2c) reveals, in contrast, slight phase errors in the multiplets which increase with greater frequency offset on a given column of the 2D matrix.

This observation suggests a dominant frequency-dependent term in the phase error φ_1 (Eqs. [4] and [9]). Although such effects are acceptable in ω_2 spectra where they only produce small-amplitude errors (*11*), they render phasing impossible in the ω_1 dimension. The origin of these phase errors is the presence of the G_1 gradient during the evolution time. They arise because the duration of the gradient pulse is long in comparison to the theoretically desirable time $t_1 = 0$ (the minimum t_1 is usually on the order of 3 μs to allow for phase switching). The usual gradient pulse duration of around a millisecond is long compared to the dwell time and therefore, whereas in a classic DQF COSY there is theoretically no signal when $t_1 = 0$ (*11*), the important chemical-shift dispersion during the G_1 gradient renders phase correction along the ω_1 dimension impossible. The only way to solve this problem is to regenerate the first data points in t_1 by backward linear prediction (*14–17*).

According to this method, each data point F_k can be expressed as a linear combination of the p following points F_{k+m}

$$F_k = \sum_{m=1}^{p} b_m F_{k+m}, \qquad [10]$$

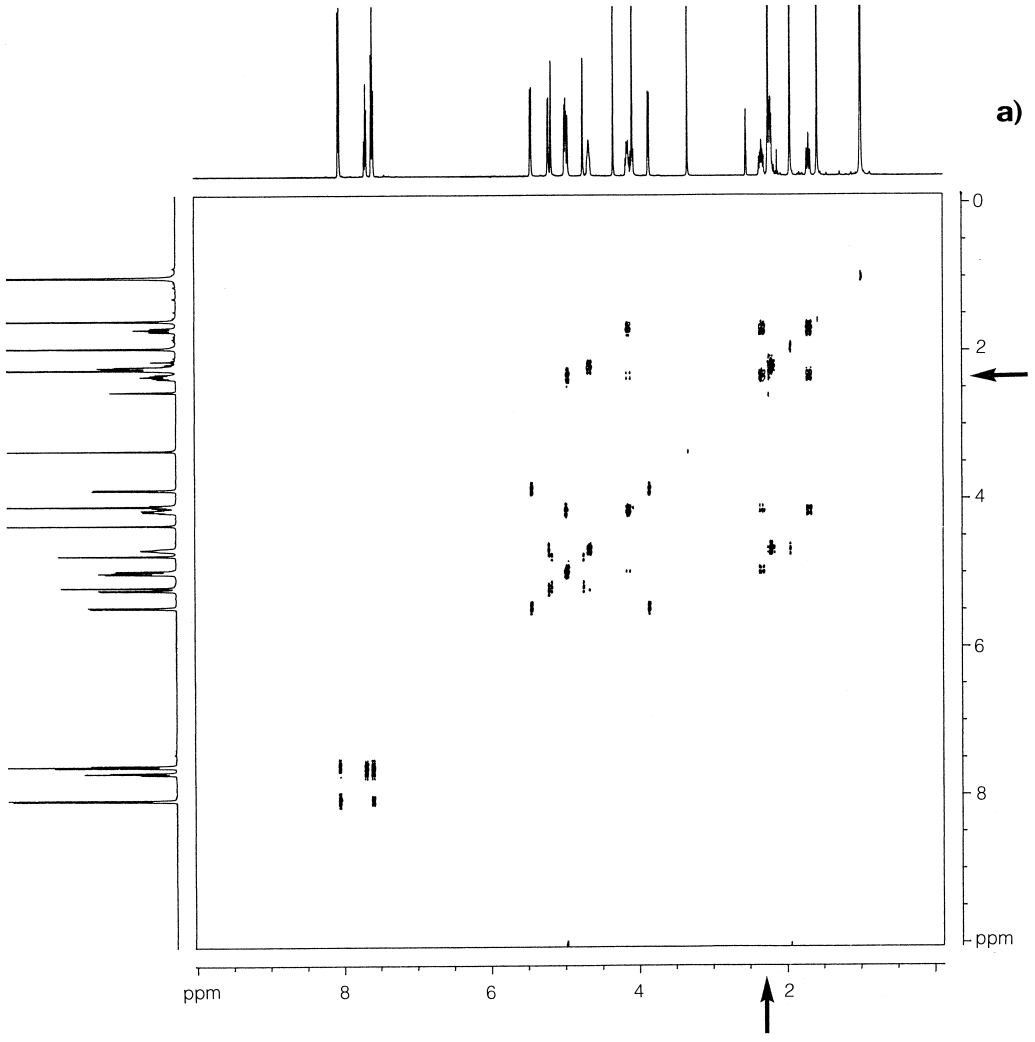

FIG. 2. (a) Two-dimensional spectrum showing elimination of rapid-scanning artifacts, (b) row at 2.34 ppm [see arrow in (a)] showing pure phase and good resolution, (c) column at the same chemical shift without linear prediction indicating frequency-dependent phase errors, and (d) removal of phase errors with backward linear prediction as described in the text.

where b_m is the mth backward coefficient which is independent of k and therefore can be determined by the existing data points by some linear calculation (*14–17*). The linear-prediction extrapolation of the missing first few points requires little computational time compared to the extensive derivation of all the spectral parameters generally performed in the conventional use of LP; moreover, because it extends the time-domain data by only a very small fraction of its total duration, the accuracy demand is not very stringent in this case, allowing the use of the fast Burg algorithm (*21*).

In the experiments described here, the initial minimum t_1 time is 1.29 ms, including the pulse width and pre- and post-gradient delays. With the 5000 Hz spectral width sampled in the ω_1 dimension according to the TPPI method, the t_1 period should be incremented by $\Delta t_1 = 1/(2 \times 5000) = 100\ \mu$s. This means that the first 12 points of all the interferograms obtained after Fourier transformation along t_2 are missing so that the lack of these data gives rise to a linear phase distortion of about 1160° across the whole spectrum. The data points were reconstructed from 22 LP coefficients using Eq. [10] while the LP coefficients b_m were determined from 44 points according to the LPBr standard Bruker routine. The same vertical trace as Fig. 2c is shown in Fig. 2d and reveals a complete suppression of phase imperfections and a slightly persistent rolling baseline for the pure-absorption spectrum in the ω_1 dimension. Indeed, despite these important phase distortions—which are certainly nonlinear—only a modest linear frequency phase correction is needed because all the signals are narrow and well separated (*16*).[1] Nevertheless, the remaining discernible undulation of the baseline should be unavoidable and cannot be properly

[1] We are indebted to the referee for pointing out this apparent contradiction to us.

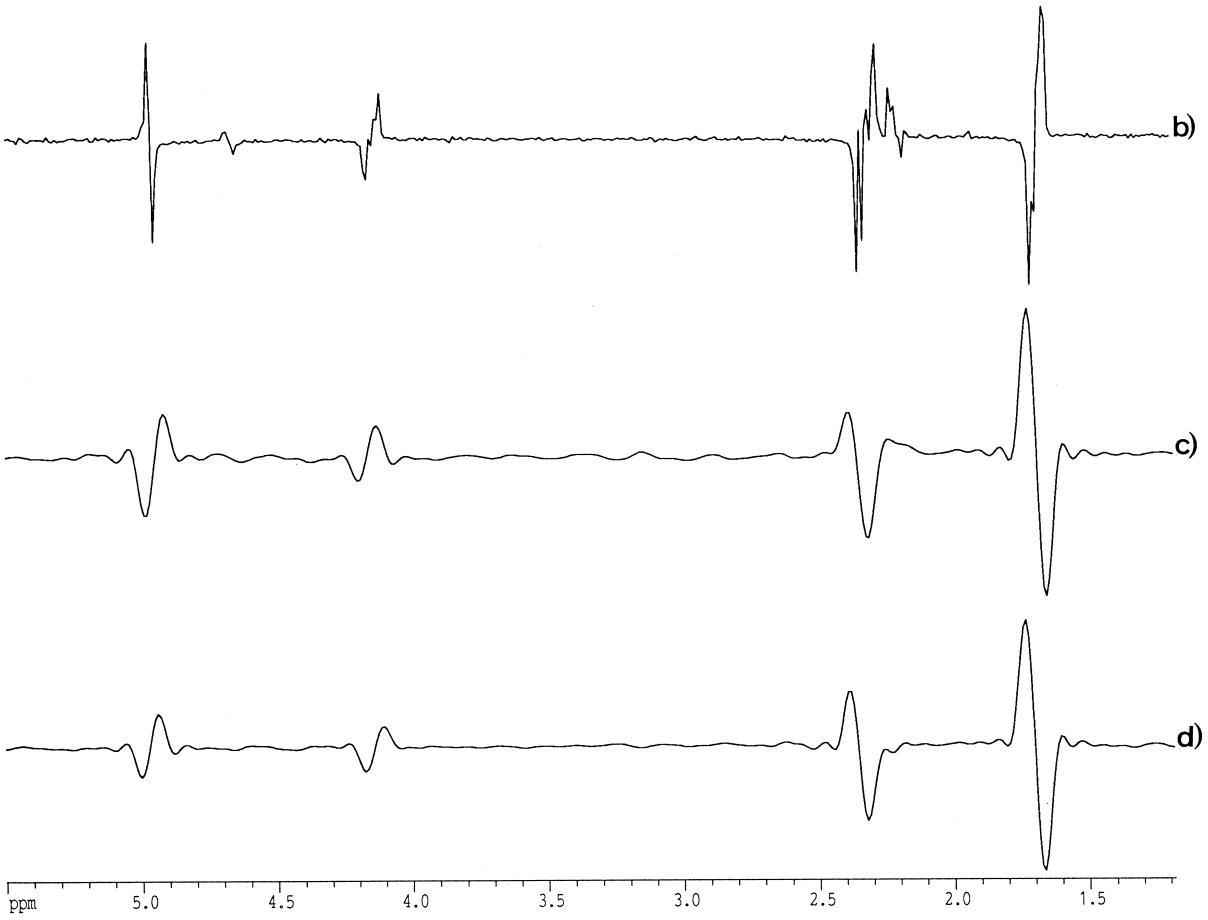

FIG. 2—*Continued*

corrected for because the interferograms can never be accurately extended to the exact point $t_1 = 0$ where all the sinusoids are in phase (*16*) (see Footnote 1). These observations provide clear evidence that the problems encountered in phasing the 2D data arise from the application of a gradient during the evolution time, which is essential for removing artifacts in GEDQF COSY experiments. As a result, the need for sampling at the beginning of each time domain is more critical in the evolution period compared to the acquisition period. Because of the irreversible frequency-dependent phase shifts which are generated, a careful backward LP reconstruction is needed to obtain good phasing along the ω_1 dimension.

Finally, it would be worthwhile to comment about the sensitivity of the method compared to (i) the phase cycled pure-phase DQF COSY and to (ii) the pure-phase absorption GEDQF COSY without any gradient in the evolution time t_1 (*3*). Such an analysis has been previously and carefully undertaken by Keeler *et al.* (*2, 3, 9*) who assume the same underlying resolution in F_1 and the same total experimental time for each of the three variants. It is clear that the need to apply a gradient during the evolution time t_1 results in a decrease by a factor of $\sqrt{2}$ in the sensitivity of our method compared to the pure-phase absorption GEDQFCOSY without any gradient in t_1 because only the coherence order $p = +1$ or $p = -1$ is selected during t_1; since this last experiment in itself already has a sensitivity poorer by a factor of $\sqrt{2}$ than the classical cycled DQFCOSY because only one of the two double-quantum coherences ± 2 is retained during the mixing time, a twofold reduction in sensitivity is expected for our method commpared to the usual pure-phase DQFCOSY. However, it should be stressed that, in our experiment, the lack of t_1 noise and artifact peaks more than compensates for the lower sensitivity.

In conclusion, the general procedure described here and in our previous note (*1*) yields artifact-free gradient-enhanced multiple-quantum-filtered spectra in absolute or pure-phase mode without the need for complicated acquisition schemes or data treatment procedures. It is our experience that the method can be easily extended along the same principles to triple-quantum-filtered TQFCOSY experiments by using a gradient combination such as $G_1{:}G_2{:}G_3 = 1{:}3{:}10$ in the evolution, mixing, and acquisition periods respectively.

REFERENCES

1. A. A. Shaw, C. Salaun, J. F. Dauphin, and B. Ancian, *J. Magn. Reson. A* **120,** 110 (1996).
2. G. Kontaxis, S. Stonehouse, E. D. Laue, and J. Keeler, *J. Magn. Reson. A* **111,** 70 (1994).
3. A. L. Davis, E. D. Laue, J. Keeler, D. Moskau, and J. Lohman, *J. Magn. Reson.* **94,** 637 (1994).
4. R. E. Hurd, B. K. John, and H. D. Plant, *J. Magn. Reson.* **93,** 666 (1991).
5. U. Piantini, O. W. Sørensen, and R. R. Ernst, *J. Am. Chem. Soc.* **104,** 6800 (1982).
6. A. J. Shaka and R. Freeman, *J. Magn. Reson.* **51,** 169 (1983).
7. M. Rance, O. W. Sørensen, G. Bodenhausen, G. Wagner, R. R. Ernst, and K. Wüthrich, *Biochem. Biophys. Res. Commun.* **117,** 479 (1983).
8. A. E. Derome and M. P. Williamson, *J. Magn. Reson.* **88,** 177 (1990).
9. A. L. Davis, J. Keeler, E. D. Laue, and D. Moskau, *J. Magn. Reson.* **98,** 207 (1992).
10. P. Bachmann, W. P. Aue, L. Müller, and R. R. Ernst, *J. Magn. Reson.* **28,** 29 (1977).
11. J. Keeler and D. Neuhaus, *J. Magn. Reson.* **63,** 454 (1985).
12. G. Drobny, A. Pines, S. Sinton, D. P. Weitekamp, and D. Wemmer, *Faraday Symp. Chem. Soc.* **13,** 49 (1979).
13. D. Marion and K. Wüthrich, *Biochem. Biophys. Res. Commun.* **113,** 967 (1983).
14. D. S. Stephenson, *Prog. NMR Spectrosc.* **20,** 515 (1988).
15. R. de Beer and D. van Ormondt, *NMR Basic Princ. Prog.* **26,** 201 (1992).
16. (*a*) H. Gesmar and J. J. Led, *J. Magn. Reson.* **76,** 183, 575 (1988); **83,** 53 (1989); (*b*) J. J. Led and H. Gesmar, *Chem. Rev.* **91,** 1413 (1991); *J. Biomol. NMR* **1,** 237 (1991); (*c*) H. Gesmar, J. J. Led, and F. Abildgaard, *Prog. NMR Spectrosc.* **22,** 255 (1990).
17. (*a*) D. Marion and A. Bax, *J. Magn. Reson.* **83,** 205 (1989); (*b*) G. Zhu and A. Bax, *J. Magn. Reson.* **90,** 405 (1990); **98,** 192 (1992); **100,** 202 (1992).
18. R. R. Ernst, G. Bodenhausen, and A. Wokaun, ''Principles of Nuclear Magnetic Resonance in One and Two Dimensions,'' Clarendon Press, Oxford, 1987.
19. J. Ruiz Cabello, G. W. Vuister, C. T. W. Moonen, P. Van Gelderen, J. S. Cohen, and P. C. M. Van Zijl, *J. Magn. Reson.* **100,** 282 (1992).
20. M. H. Levitt and R. Freeman, *J. Magn. Reson.* **33,** 473 (1979).
21. W. H. Press, B. P. Flannery, S. A. Tenkolsky, and W. T. Vetterling, *in* ''Numerical Recipes: The Art of Scientific Computing,'' Chap. 12, Cambridge Univ. Press, Cambridge, 1989.